Absorption Spectroscopy Characterization Measurements of a Laser-produced Na Atomic Beam

C.H. Ching, J.E. Bailey, P.W. Lake, A.B. Filuk, R.G. Adams, and J. McKenney

Sandia National Laboratories, Albuquerque, New Mexico 87185

This work describes a pulsed Na atomic beam source developed for spectroscopic diagnosis of a high-power ion diode. The goal is to produce a ~ 10^{12}-cm^{-3}-density Na atomic beam that can be injected into the diode acceleration gap to measure electric and magnetic fields from the Stark and Zeeman effects through laser-induced-fluorescence or absorption spectroscopy. A ~ 10 ns fwhm, 1.06 μm, 0.6 J/cm^2 laser incident through a glass slide heats a Na-bearing thin film, creating a plasma that generates a sodium vapor plume. A ~ 1 μsec fwhm dye laser beam tuned to 5890 Å is used for absorption measurement of the Na I resonant doublet by viewing parallel to the film surface. The dye laser light is coupled through a fiber to a spectrograph with a time-integrated CCD camera. A two-dimensional mapping of the Na vapor density is obtained through absorption measurements at different spatial locations. Time-of-flight and Doppler broadening of the absorption with ~ 0.1 Å spectral resolution indicate that the Na neutral vapor temperature is about 0.5 to 2 eV. Laser-induced-fluorescence from ~ 1 x 10^{12}-cm^{-3} Na I 3s-3p lines observed with a streaked spectrograph provides a signal level sufficient for ~ 0.06 Å wavelength shift measurements in a mock-up of an ion diode experiment.

I. Introduction

Visible spectroscopy has been used to study the charged-particle dynamics in a high-power ion diode on the Particle Beam Fusion Accelerator II (PBFA II) at Sandia National Laboratories[1,2]. Knowledge of the charged-particle distribution across the diode acceleration gap can enhance

the understanding of the ion current density attainable for a given species, the ion-beam divergence, and various diode electromagnetic instabilities. However, this "passive" spectroscopy which uses emission from naturally-occurring, low-density charge-exchange lithium neutral atoms, limits the mid-gap measurements to the time after lithium atoms travel from the anode across the gap. In addition, Doppler broadening of these energetic lithium neutrals mask the Zeeman splitting, preventing magnetic field measurements, and relatively-small Li I 2s-2p Stark shift inhibits accurate electric field measurements below ~ 2 MV/cm. These limitations can be overcome using an Active Spectroscopy Probe (ASP). This probe has three components: injection of an alkali neutral atom beam into the diode, excitation by dye laser tuned to resonance transitions, and observation of the fluorescence using 2-D space- and time-resolved spectroscopy. The localized excited neutrals provide a third spatial resolution dimension, the low Doppler broadening enables resolution of the individual Stark and Zeeman components, and the freedom to place desired atoms at specific locations enables measurements of both small and large fields throughout the experiment. This proposed method is similar to a technique that has already been demonstrated in a low-power electron beam diode. Note that the Stark-Zeeman pattern can also be observed with absorption spectroscopy.

Diagnosing the PBFA II ion diode requires an injected-neutral atom density in the range of 10^{12} to 10^{13} cm^{-3} for good signal-to-noise ratio in ~ 1 nsec from a ~ 5 mm^3 volume, since the photon collection efficiency is limited to $\leq 5 \times 10^{-5}$ by the diode geometry. These densities are too low to have significant ionization effects on the diode pulse timescale[3] if the other contaminant neutrals, electrons, ions are not injected along with the sodium. This paper will address the density issue only and additional measurements are needed to study plasma and other neutral species generated. Sodium is chosen because its resonance lines can be readily probed with LIF

(Laser-Induced-Fluorescence) or absorption and the Stark shift for the Na I 3s-3p lines is large enough to measure ~ 0.5 MV/cm, but not so large that the neutrals would field ionize[4]. In addition, we don't want to use lithium since we want to be able to distinguish between gap neutrals and injected neutrals. Laser ablation production of neutral atom beam has been extensively developed for a variety of applications, including basic atomic physics, magnetic fusion, and electron beam diode research[5-8]. Density measurements were carried out with time-of-flight laser-induced-fluorescence[9,10]. However, most of these previous works used in-situ deposited metals as a source and had no spatial information about the density distribution.

II. Experimental Apparatus and Results

A schematic of the experimental apparatus is shown in Figure 1. A Nd:YAG laser producing 0.6-0.7 J/cm^2, ~ 10 ns fwhm pulse at λ = 1.06 μm is used to irradiate a coated target from the rear side. The beam is expanded and passed through a beam homogenizer[10] to provide approximately ± 10% intensity uniformity illumination on the target. The spot size on target is 6 x 6 mm. The target is a fused-silica glass slide with 700 Å thick vanadium film vacuum-evaporated onto the front side, followed by a 1000-3000 Å thick NaF or NaAu film. NaF is easy to fabricate but the Na atoms may be accompanied by F atoms or NaF molecules. A NaAu alloy was therefore fabricated. The NaAu film is sputter-deposited on top of the vanadium thin film by a standard two inch diameter pure gold sputter target filled with three channels of resolidified pure sodium. The resultant NaAu thin film is a stable, consistent binary alloy due to the atom-by-atom vapor phase sputter-deposition process[12]. These NaAu targets have excellent cosmetics and have a Na:Au film ratio of 1:1.77. The purpose of the vanadium is to increase absorption of the 1.06 μm Nd:YAG laser light at the metal-glass interface. This geometry is preferred because

it is difficult to implement front side illumination inside the diode gap and rear-side illumination is believed to generate neutrals more efficiently[5]. The target is mounted on a three-way translational stage which can be moved in a plane perpendicular to the laser beam so that a number of spots can be irradiated without breaking vacuum. The base pressure inside the vacuum system is less than 5×10^{-6} Torr. A flashlamp-pumped dye laser with a ~ 1 μsec fwhm laser beam tuned to 5890 Å (with Rhodamine 590 dye) with 37 Å fwhm bandwidth is used for absorption measurements. The dye laser fluence is maintained ≤ 0.1 mJ/cm^2 to avoid saturation effects. The beam passes through the side window of the chamber parallel to the front surface of the target and goes directly to the collecting lens and fiber. Collimated light is collected from a 6-mm-diameter, nearly-cylindrical, region at the target midplane, and transmitted through a 400-μm-diameter fiber to a 1-m Czerny-Turner spectrograph with a time-integrated CCD camera located in the exit focal plane. A 2400-line/mm holographic grating provides a spectral resolution of ~ 0.08 Å. Time- and space-resolved absorption measurements are set by the pulse width (~ 1 μsec) of the dye laser beam and collecting region (~ 6 mm) of the apertured fiber. By translating both the dye laser beam and the collecting fiber simultaneously to different spatial locations with respect to the target, a two-dimensional mapping of the Na vapor density can be obtained. A copper plate, shown in Figure 1, is installed about 7 cm downstream from the target to reproduce the effect of the actual PBFA II anode on the neutral density. It is possible that the anode " wall" reflects neutral atoms and increases Na density. In addition, a 6 x 6 mm or a 2 x 2 cm aperture is installed ~ 3 cm from the target to reduce the spread of the neutral beam.

Figure 2 shows a typical absorption spectrum. A single Gaussian fit is performed for each spectral line, with the wavelength uncertainty determined from the fluctuation level of the data about the fit using experimentally-verified Gaussian statistics[13]. The spectral line strength and

spectral width are obtained from the fitting program. The fractional absorption of the line is proportional to the value of the line strength divided by the background continuum intensity and the spectral width. The density is determined from the observed fractional absorption using a computer routine that integrates over the observed spectral width using the Voigt profiles, assuming the Gaussian width is much greater than the Lorentzian width. The routine also calculates the expected fwhm of the absorption feature, for a given instrument width and vapor cloud temperature, including the effect of absorption saturation. The instrument-width blurring effect on the absorption shape is included, since this might alter the amount of absorption within $\pm \Delta\lambda/2$. This absorption fraction is a modification of Mitchell and Zemansky's[14], because, in practice, the Doppler width and instrument width may be comparable. Figure 3 shows the calculated fractional absorption and absorption feature spectral width versus atomic line density obtained from the routine at different neutral vapor temperature. At low line densities the fractional absorption is sensitive to line density but almost independent of temperature. At higher line densities the measured width may be used to determine the line density if the neutral temperature is known from Doppler broadening. Time-of-flight and Doppler broadening of the absorption indicate that the Na neutral vapor temperature is about 0.5 to 2 eV. Figure 4 shows the Na neutral line-density versus delay time (measured with respect to the incident YAG laser pulse) for Na I at 5890 Å, observed at 6 cm from the target. We are using the 5890 Å line only because the smaller oscillator strength results in less absorption, providing more accurate measurements when absorption saturation is important. A 2 x 2 cm aperture and a copper plate are used. Comparison of the two targets (3000 Å thick NaF and 1100 Å thick NaAu) indicates that the relatively-low-density foot from the 3000 Å thick NaF target travels faster than from NaAu, but the bulk (higher density) part travels at about the same speed. The approximate path length for absorption in this case is about 2-2.5 cm for the 2 cm aperture. Figure 5 shows the

two-dimensional mapping of the neutral density distribution with the 2 cm aperture. Higher neutral line-densities are observed closer to the targets. In addition, neutrals propagate about two times faster perpendicular to the target surface than parallel to the target, and the neutrals produced by different thicknesses of NaF are comparable at the same time and same location. Figure 6 shows the distribution of the neutrals with the 6 mm aperture. Note that the delay time is longer (3.2 μsec as compared to 2.7 μsec as in Figure 5) to compensate for the reduction of neutrals due to the reduced aperture. With the 6 x 6 mm aperture, we could improve the density measurements by reducing the path length and mimic conditions in diode experiments where control spread of the injected neutral beam is needed.

Using the knowledge gained in the absorption measurements, an integrated test was done to demonstrate the feasibility of using this atomic source on an ion diode. Laser-induced-fluorescence was observed at 5-6 cm from the target with the 6 mm aperture, using 0.6 J/cm^2 of Nd:YAG fluence. Figure 6 shows that a Na neutral of ~ 1 x 10^{12} cm^{-2} line-density (corresponding to roughly 1 x 10^{12} cm^{-3} density for ~ 1 cm path length) was present in the fluorescing volume. The collection optics was rotated about 30 degree from the dye laser beam path to avoid stray light from the beam. And the dye laser fluence was increased to ~ 10 mJ/cm^2 to ensure saturation of the transition. The Na I resonance-fluorescence doublet lines were recorded on film with the MCP-intensified streak spectrograph. Lineouts over 1 ns were taken from the digitized film and the spectra were fit as mentioned earlier. After correcting for image distortion, the sample variance of the Na I peaks about their mean wavelengths gave an estimated 1-standard-deviation wavelength uncertainty of less than 0.06 Å. In a diode experiment we expect each line to be split into numerous components by Stark and Zeeman effects, so the uncertainty in a single component's wavelength would be greater than the above

value. Nevertheless, this very low uncertainty is a good indication that the technique should work to resolve 1-3 Å Zeeman splits and 0.3-35 Å Na Stark shifts expected in our ion diodes.

Acknowledgment
This work was supported by the U.S. Department of Energy under contract No. DE-AC04-94AL85000.

References

1. J.E. Bailey et al., Phys. Rev. Lett. **74**, 1771 (1995).
2. J.E. Bailey, A.L. Carlson, T.L. Morrison, and Y. Maron, Rev. Sci. Instrum. **61**, 3075 (1990); J.E. Bailey, A.L. Carlson, and P. Lake, in Proceedings of the 1994 IEEE International Conference on Plasma Science, Santa Fe, 1994 (IEEE Report No. 94CH3465-2, 1994), p.133.
3. Dale Welch
4. Y. Maron, Weizmann Institute of Science (private communication).
5. J.F. Friichtenicht, Rev. Sci. Instr. **45**, 51 (1974).
6. S.P. Tang, N.G. Utterback and J.F. Friichtenicht, J. Chem. Phys. **64**, 3833 (1976).
7. E.S. Marmar, J.L. Cecchi and S.A. Cohen, Rev. Sci. Instrum. **46**, 1149 (1975).
8. B.A. Knyazev, S.V. Lebedev, and K.I. Mekler, Sov. Phys. Tech. Phys. 31 (7), 773 (1986).
9. J.S. Bakos, I.B. Foldes, P.N. Ignacz, G. Kocsis, J. Szigeti and J. Kovacs, Optics Comm. **74**, 374 (1990).
10. Y.T. Lie, A. Pospieszczyk, and J.A. Tagle, Fusion Technology. **6**, 447 (1984).
11. L.P. Schanwald, Sandia National Laboratories, Report SAND89-0717, (1989). Available from NTIS.
12. H. Okamoto and T.B. Massalski, eds., *Phase Diagram of Binary Gold Alloys* (ASM International, 1987).
13. R.L. Coldwell and G.J. Bamford, *The Theory and Operation of Spectral Analysis Using ROBFIT* (AIP, New York, 1991).
14. A. Mitchell and M. Zemansky, *Resonance Radiation and Excited Atoms* (Macmillan, 1934).

Figure Captions

Figure 1. A schematic of experimental apparatus.

Figure 2. A typical absorption spectrum showing the Na I resonance doublet.

Figure 3. Fractional FWHM-averaged absorption (solid) and FWHM (dashed) versus line density at vapor temperatures 0.5, 1.0, 1.5 and 2.0 eV for Na I 5890 Å (instrument width = 0.08 Å).

Figure 4. Na neutral line-density versus delay time. A 2 x 2 cm aperture (at 3 cm) and the copper plate (at 7 cm) are used for Na I 5890 Å observed 6 cm from the target. 3000 Å thick NaF target (O) and 1100 Å thick NaAu target (●).

Figure 5. Na neutral line-density versus transverse position, from various distances x from target. Na I 5890 Å is used without aperture. 3000 Å thick NaF target at delay time 2.7 μsec, x = 6.0 cm (O), 4.0 cm (●) and 2.5 cm (▽). 1100 Å thick NaAu target at delay time 3.5 μsec, x = 6.7 cm (▼), 4.7 cm (□) and 2.7 cm (■). 1410 Å thick NaF target at delay time 2.7 μsec, x = 6.1 cm (Δ) and 4.0 cm (▲).

Figure 6. Na neutral line-density versus transverse position. Na I 5890 Å is used the copper plate and a 6 x 6 mm aperture. 3000 Å thick NaF target at delay time 3.2 μsec, x = 6.0 cm (O). 1000 Å thick NaAu target at delay time 4.0 μsec, x = 6.0 cm (●).

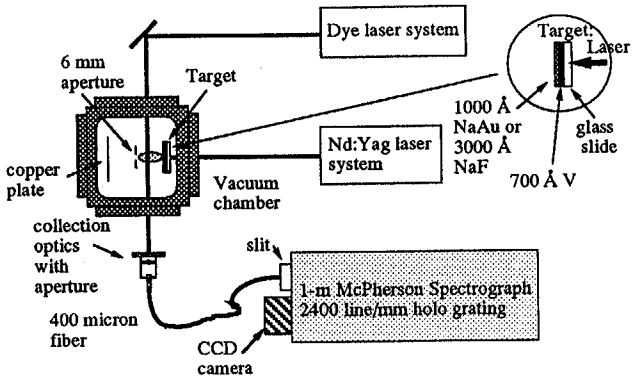
Dye laser system
Target:
Laser
6 mm
aperture
Target
1000 Å
NaAu or
3000 Å
NaF
glass
slide
Nd:Yag laser
system
copper
plate
Vacuum
chamber
700 Å V
collection
optics
with
aperture
slit
1-m McPherson Spectrograph
2400 line/mm holo grating
400 micron
fiber
CCD
camera

Figure 1

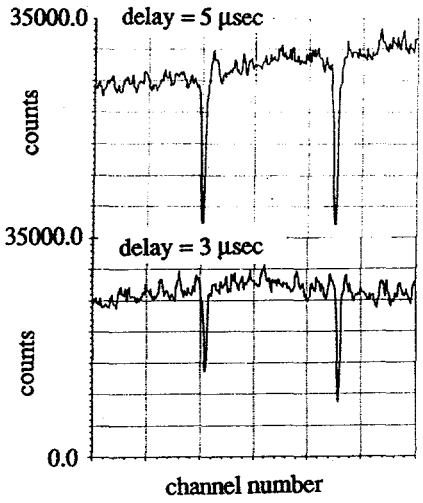
35000.0
delay = 5 µsec
counts
35000.0
delay = 3 µsec
counts
0.0
channel number

Figure 2

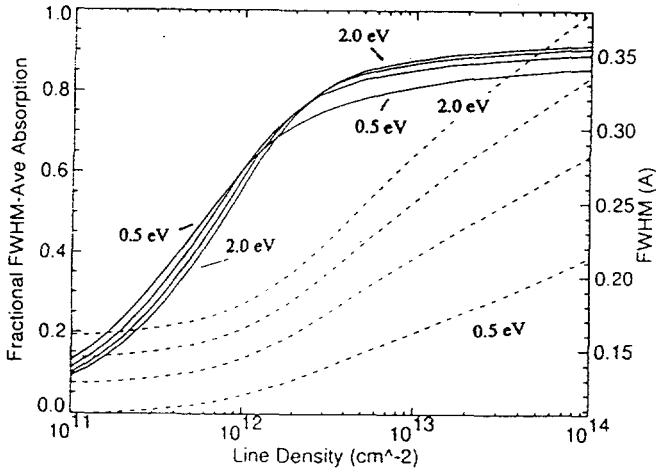
1.0
0.8
0.6
0.4
0.2
0.0
Fractional FWHM-Ave Absorption
0.35
0.30
0.25
0.20
0.15
FWHM (A)
2.0 eV
0.5 eV
2.0 eV
0.5 eV
2.0 eV
0.5 eV
10^{11}
10^{12}
10^{13}
10^{14}
Line Density (cm^-2)

Figure 3

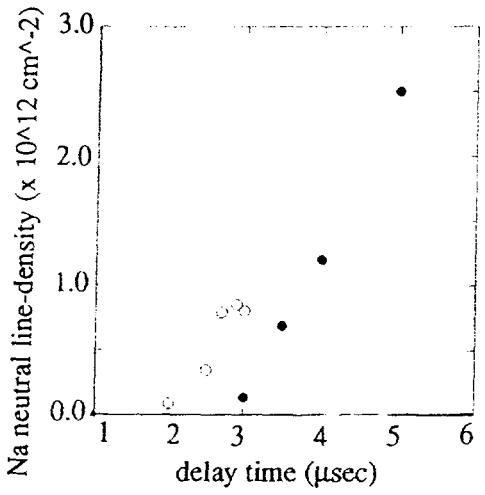
Na neutral line-density (x 10^12 cm^-2)
3.0
2.0
1.0
0.0
1
2
3
4
5
6
delay time (μsec)

Figure 4

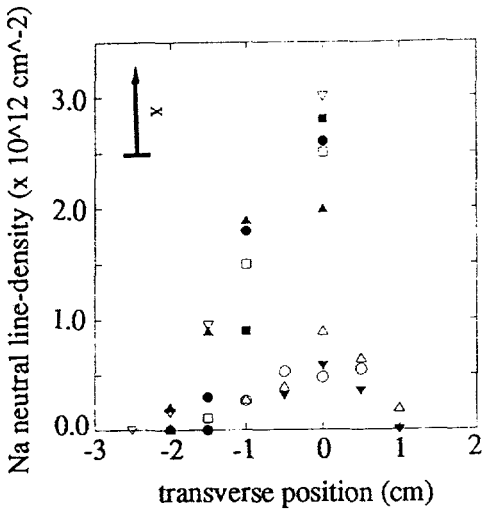
Na neutral line-density (x 10^12 cm^-2)
3.0
2.0
1.0
0.0
x
-3
-2
-1
0
1
2
transverse position (cm)

Figure 5

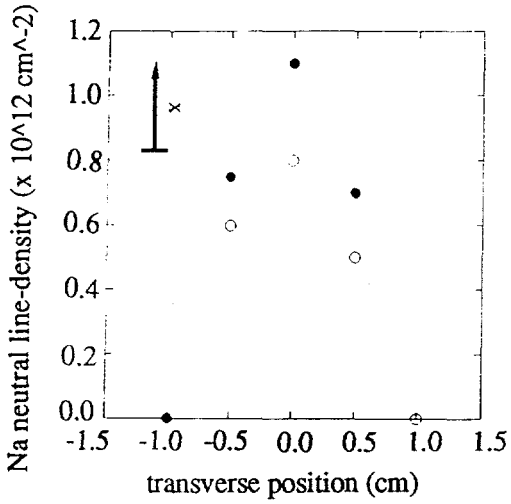
Na neutral line-density (x 10^12 cm^-2)
1.2
1.0
0.8
0.6
0.4
0.2
0.0
x
-1.5
-1.0
-0.5
0.0
0.5
1.0
1.5
transverse position (cm)

Figure 6